J Mater Sci (2009) 44:2820–2827
DOI 10.1007/s10853-009-3372-4

Synthesis and characterization of anodized titanium-oxide nanotube arrays

Michael Z. Hu · Peng Lai · M. S. Bhuiyan · Costas Tsouris · Baohua Gu · M. Parans Paranthaman · Jorge Gabitto · Latoya Harrison

Received: 23 October 2008 / Accepted: 23 February 2009 / Published online: 25 March 2009

Abstract Anodized titanium-oxide containing highly ordered, vertically oriented TiO_2 nanotube arrays is a nanomaterial architecture that shows promise for diverse applications. In this paper, an anodization synthesis using HF-free aqueous solution is described. The anodized TiO_2 film samples (amorphous, anatase, and rutile) on titanium foils were characterized with scanning electron microscopy, X-ray diffraction, and Raman spectroscopy. Additional characterization in terms of photocurrent generated by an anode consisting of a titanium foil coated by TiO_2 nanotubes was performed using an electrochemical cell. A platinum cathode was used in the electrochemical cell. Results were analyzed in terms of the efficiency of the current generated, defined as the ratio of the difference between the electrical energy output and the electrical energy input divided by the input radiation energy, with the goal of determining which phase of TiO_2 nanotubes leads to more efficient hydrogen production. It was determined that the anatase crystalline structure converts light into current more efficiently and is therefore a better photocatalytic material for hydrogen production via photoelectrochemical splitting of water.

Introduction

Anodized titanium-oxide (ATO) containing highly ordered, vertically oriented TiO_2 nanotube arrays has been considered as an important nanostructure platform for various applications, including solar cells, sensors, catalysts, and devices for the generation of hydrogen by water photoelectrolysis [1, 2]. The nanoporous nature of ATO offers a large internal surface area without concomitant decrease in geometrical and structural order. The orientation of crystalline nanotube arrays provides excellent electron percolation pathways for vectoral charge transfer between the interfaces.

Hydrogen has been produced from water using sunlight as the energy source, but efficiencies are not high enough to allow commercial production of hydrogen on a large scale. A target hydrogen production efficiency of 10% is required for water-splitting technology to be commercially viable [3]. This goal is based on current fuel and infrastructure costs and is likely to change depending on the future economic and political conditions.

The pioneering work of Fujishima and Honda [4] showed that water splitting was possible by illuminating a TiO_2 electrode in an electrochemical cell with sunlight. Much research has been undertaken in the last three decades to engineer a suitable photocatalyst material for water splitting in an electrochemical cell. A good photocatalyst material must include the following properties: a band gap that is optimal for water splitting (approximately 2 eV band gap, with conduction and valence band edges optimally placed with respect to the water redox potentials), strong optical absorption in the visible and ultraviolet (UV) spectral regions, good stability in strong electrolytes, and efficient charge transfer properties between the semiconductor and the electrolyte [5].

Titanium dioxide is a popular photocatalyst as it is less toxic, stable, and inexpensive. The anatase and rutile phases of TiO_2 have a bandgap of 3.2 and 3.0 eV, respectively. Since only 2.7% of the solar photon flux has energy greater than 3.0 eV, the light-harvesting ability of

M. Z. Hu (✉) · P. Lai · M. S. Bhuiyan · C. Tsouris · B. Gu · M. Parans Paranthaman
Oak Ridge National Laboratory, Oak Ridge, TN 37831, USA
e-mail: hum1@ornl.gov

J. Gabitto · L. Harrison
Chemical Engineering Department, Prairie View A and M University, P.O. Box 4229, Prairie View, TX 77446-4229, USA

TiO_2 is very limited. The maximum practical efficiency for hydrogen production using TiO_2 is below 0.5%, far from the target of 10% [5]. There have been numerous attempts to reduce the bandgap of TiO_2 and to shift the absorption to longer wavelengths in order to increase the water-splitting efficiency. Some promising techniques include doping the TiO_2 with nitrogen [6] or carbon [7], and producing composite electrodes by including materials with a narrower bandgap, such as metal sulfides [8]. Tungsten trioxide has been recently considered as a new photoanode material or mixture material with TiO_2 for water splitting because it can offer a relatively small band gap of 2.5 eV and corrosion stability in aqueous solutions [9].

The principal impetus toward fabricating nanodimensional materials lies in the promise of achieving unique properties and superior performance due to their inherent nanoarchitectures. Since the pioneering work of Fujishima and Honda [4], vertical electrodes have been used in electricity and/or hydrogen producing devices from TiO_2. New nanomaterials are currently designed to adapt to the existing device architectures. The nanotube structure increases the surface area for electrolyte–electrode contact compared to random porous structures, and also maximizes the light absorption rate. There have been several attempts to fabricate ordered TiO_2 nanotube arrays by anodization of thick or thin films of titanium [10]. Titanium dioxide nanotubes fabricated by anodization are highly ordered, high-aspect-ratio structures with nanocrystalline walls oriented perpendicular to the substrate. The nanotubes have a well-defined and controllable pore size, wall thickness, and tube length. The nanotube arrays demonstrate unique material properties; for example, TiO_2 nanotube array-based resistive gas sensors exhibit an amazing 1,000,000,000% change in electrical resistance upon exposure to 1000 ppm of hydrogen gas at 23 °C [11, 12].

Titanium dioxide exists in three different crystalline structures: anatase, rutile, and brookite. The anatase structure has attracted much attention over the last few decades for its technological applications. Titanium dioxide in the anatase phase exhibits a high photocatalytic activity, which is promising for the applications proposed for such areas as environmental purification, decomposition of carbonic acid gas, and generation of hydrogen gas by decomposing water using solar energy [13, 14].

The electrolyte composition and applied anodic potential primarily determine the oxide nanostructure resulting from anodization. Sulfuric acid has been the most widely used electrolyte for nonporous TiO_2 films formed at lower potentials. Porous TiO_2 films can be formed at higher potentials due to electrical breakdown of the oxide [15, 16]. In fluoride-containing electrolytes, the anodization of titanium is accompanied by the chemical dissolution of TiO_2 due to the formation of TiF_6^{2-}.

Highly ordered nanotube arrays, in place of porous or nonporous structures, are formed at relatively low potentials (e.g., 10 V) as a result of the competition between the electrochemical etching and the chemical dissolution [17]. These arrays were reported to be obtained only in either fluoride-containing acids [16] or in a mixture of fluoride-containing acids and other acids, including sulfuric acid [17] and acetic acid [18]. Since the high rate of chemical dissolution of the oxide in electrolytes containing hydrofluoric acid is the factor directly limiting the nanotube length, our efforts have been focused on controlling the dissolution rate by adjusting the pH of the electrolyte through additives and by using different fluorine-containing salts, such as KF and NaF instead of HF.

Potassium fluoride is totally dissociated in water, with F^- hydrolyzing with water to form HF:

$$F^- + H_2O = HF + OH^- \quad (1)$$

Therefore, a KF electrolyte, without the addition of other acids, will result in an alkaline solution. The ultimate concentrations of F^- and HF are determined by the pH of the solution. Prior to the addition of KF, the electrolyte pH was adjusted by adding sodium hydroxide, sulfuric acid, sodium hydrogen sulfate, citric acid, and in one case, phosphoric acid. By optimizing the anodization conditions, highly ordered nanotube arrays were produced that were approximately 6.0 μm in length, an order of magnitude longer than the previously reported arrays [18].

In this paper, films that contain TiO_2 nanotube arrays on titanium foils were synthesized by anodization in HF-free aqueous solutions; anatase and rutile phases were obtained by annealing under controlled temperatures. Analyses by scanning electron microscopy (SEM), X-ray diffraction (XRD), and Raman spectroscopy were conducted on the various synthesized and annealed ATO samples. Then studies on photoelectrochemical water splitting were carried out with various phases of anodized TiO_2 for potential application in photocatalytic hydrogen production.

Experimental

Preparation of anodized TiO_2 nanotube arrays

The original titanium films in this work were prepared from 2.54 × 2.54 cm metallic titanium foils (0.127 mm thick, Alfa Aesar). Two DC power supplies (6615A 0-60V/0-9A and 6653A 0-35V/0-15A) were used for the anodization process under current-limiting conditions, with a Pt plate as the cathode and Ti foil as the anode. The HF-free aqueous electrolyte solution contains 1 M $(NH_4)_2SO_4$ plus 0.5 wt% NH_4F [i.e., 132.05 g of $(NH_4)_2SO_4$ and 5.25 g of NH_4F in 1 L of deionized water]. Ammonium sulfate was purchased

from Fisher Scientific (purity 99.9%; F.W. 132.14); ammonium fluoride was purchased from J. T. Baker (Lot T03668; purity 99.0%; F.W. 37.04). The anodization involved electrochemical oxidation of titanium into amorphous TiO_2 and chemical dissolution of the oxide into soluble titanium fluoride species (TiF_6^{2-}):

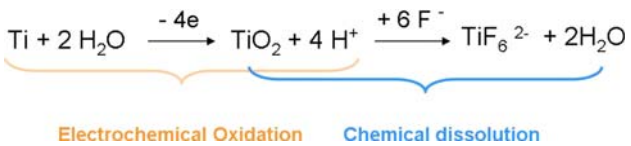

In this reaction, $H_2O + 2e^- \rightarrow \frac{1}{2}O_2 + 2H^+$, so the dissolution of oxide occurring due to local acidity at the bottom of the TiO_2 nanotube leads to the progressive growth of nanotube length.

The synthesis parameters that affect the anodization include applied voltage, initial current, voltage sweep rate (i.e., the rate to increase voltage from zero to the target voltage), concentration of F^-, temperature, and anodization time. A typical anodization procedure involves the following steps: (1) the Ti foil and Pt plate are ultrasonically cleaned with acetone, isopropanol, ethanol, and deionized water; (2) after the Ti foil and Pt plate are dried, they are clipped onto the electrodes of a power supply and positioned in parallel with an interspacing of $\sim$2 cm; (3) a Teflon container is filled with 50 mL of electrolyte solution, and the parallel Ti foil and Pt plate are submerged in the solution without stirring; (4) target anodization potential and initial current are set to 20 V and 0.020 A, respectively; (5) the power supply is turned on, and the anodization is carried out at room temperature ($\sim$22°C); (6) anodization continues for 6 h (usually during anodization, the Ti foil surface turns colorful and dark with time); (7) at the end of the anodization process, the Ti foil surface is rinsed several times with deionized water; and (8) the unwanted surface deposits or leftover particles are removed by ultrasonication in deionized water for about 1 min, and then the samples are dried in air. For SEM imaging, a small slice of the ATO foil was cut off and glued onto the SEM sample holder with conductive carbon paste.

Experimental analyses of ATO samples

SEM imaging was conducted using a Hitachi S-4700 instrument. Nucleation and growth of anodized TiO_2 were analyzed by in situ high temperature XRD (HT-XRD). The as-anodized sample of TiO_2 was heated from room temperature to 800 °C at a heating rate of 400 °C/min in an inert atmosphere of argon, and the θ–2θ XRD patterns were recorded at 30, 300, 400, 500, 550, 600, 650, 700, 750, and 800 °C. For the growth test, as-anodized TiO_2 was heated to 500 °C with the same heating ramp and atmosphere. Then XRD patterns were recorded for every 5 min for half an hour. Structure analysis was done by a room temperature powder XRD analysis.

Raman spectra were obtained using a Renishaw micro-Raman system (Renishaw Inc., New Mills, UK) equipped with a 300 mW near-infrared diode laser for excitation at a wavelength of 785 nm. The laser beam was set in position with a 50×, 0.5 numerical aperture Leica microscope objective at a spatial resolution of $\sim$2 μm. The laser power was $\sim$60 mW at the exit of the objective [19].

Electrochemical measurements

The water-splitting efficiency of a photocatalytic electrode can be experimentally measured using a three-electrode electrochemical cell, as shown in Fig. 1. This electrochemical cell consists of a working electrode, a platinum counter electrode, and an Ag/AgCl reference electrode. The electrodes are immersed in an electrolyte solution (1 M Na_2SO_4) contained in a cell fitted with a quartz window. An Ag/AgCl reference electrode in saturated KCl (Metrohm AG) was employed for electrochemical measurements in this work. According to the manufacturer's calibration, this reference electrode has a potential of +197 mV versus a normal hydrogen electrode (NHE) at 25 °C. Three square film samples, 1″ by 1″ in size with an active area of approximately 4 cm^2, composed of amorphous, anatase, and rutile phases, were used as the anode electrode in these photoelectrochemical studies. Electrochemical measurements were obtained for both dark and under illumination conditions.

Prior to the electrochemical measurements, the electrodes were activated by evolving hydrogen under a

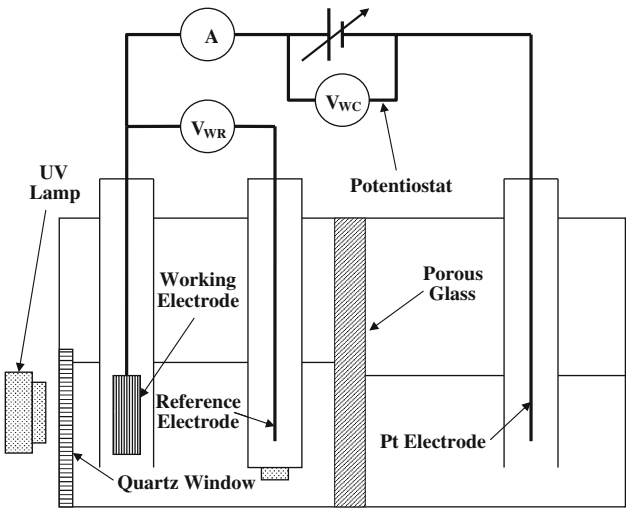

Fig. 1 Schematic representation of the three-electrode cell used for the photoelectrochemical characterization of titania nanotubes

potential of approximately 1.4 V for about half an hour. The same electrolyte as in the photoelectrochemical experiments was used. This treatment eliminated any surface contamination and activated the electrode surface.

A 1 M sodium sulfate solution was used in our experiments. The ions in the sodium sulfate solution do not interfere with the reactions on the electrodes due to their high potentials, unlike the ions in chloride solutions, for example, which form chlorine gas at the anode. The electrolyte was mechanically stirred during some experiments. No appreciable differences were found in experiments conducted under the same conditions with and without stirring.

UV sunlight was simulated by using an Oriel 6271 mercury lamp. A nominal characterization of the light intensity can be done by setting the voltage and intensity of the lamp to constant values. The power density of the incident light (I_o) corresponding to given nominal values was determined using a light meter placed inside the electrochemical cell at the anode position without the electrolyte. Table 1 shows the light intensity measurement results.

The following experimental procedure was used. First, we set the desired power in the UV lamp. Second, we set the desired voltage using a potentiostat. One can conduct dynamic scans, at a fixed scan rate, or steady-state measurements. We used steady-state measurements in this work. After applying a given voltage, we recorded the photocurrent changes until steady-state was achieved. The system showed evidence of hysteresis. Therefore, it was important to obtain two sets of measurements: one in the direction of increasing applied potential (anodic scan) and another in the direction of decreasing applied potential (cathodic scan). In these experiments, it was easier to reach steady-state conditions using decreasing scans rather than increasing scans. The two sets of data showed significant differences sometimes. Steady-state data normally agree regardless of the scan direction. However, it took more time to reach steady-state in the case of continuously increasing potential than in the case of continuously decreasing potential. A good discussion about such observations can be found in Torres et al. [6].

Table 1 Relationship between lamp power and light intensity

Current (A)	Voltage (V)	Lamp power (W)	I_o (mW/cm^2)
6	25	150	396
6	23	138	354
5	22	110	262
5	20	100	231
4	22	88	195
4	20	80	172
3	21	63	125
2	20	40	68
1	18	18	24

Once steady-state was achieved, we recorded the overall voltage, current intensity, and anodic voltage with respect to the reference electrode. The dark current values were determined in the same conditions, but without illumination. The open circuit voltage was determined by measuring the applied voltage after setting the circulating photocurrent to zero.

The efficiency, η, of the water-splitting reaction was determined using the equations proposed by Khan et al. [7]. The photoconversion efficiency (η) of light energy to chemical energy in the presence of an externally applied potential (E_{app}) can be expressed as,

$$\eta = \{\text{Total power output} - \text{Electrical power input}\}/\text{Light power input}, \quad (2)$$

or

$$\eta = \{J_p[1.23\,\text{V} - E_{app}]/I_o\} \quad (3)$$

where J_p is the photocurrent density, defined as the measured current density under illumination minus the dark current at the same applied voltage; 1.23 V is the potential corresponding to the Gibbs free energy change per electron for water-splitting reaction; $E_{app} = E_{mea} - E_{aoc}$. E_{mea} is the working electrode potential relative to the reference electrode under illumination; E_{aoc} is the electrode potential at open circuit condition in the same electrolyte solution and under the same illumination of light at which was measured; and I_o is the flux of incoming radiation experimentally measured [7].

Results and discussion

SEM examination

The surface morphology of the nanostructures formed in the anodized films, as observed from the SEM micrographs is shown in Fig. 2. The as-anodized TiO_2 film shows good arrays of nanotubes (80 nm in diameter and $\sim$0.5 μm in thickness, Fig. 2a, b). After annealing at 500 °C in flowing of Ar gas at 1 atm for 30 min, the morphology of the nanotubes was still maintained (Fig. 2c). However, after annealing at 800 °C in Ar for 30 min, the nanotube array structure had been transformed into crystalline pores with random orientation (Fig. 2d).

Nucleation and growth analysis by in situ HTXRD

The structure of the as-anodized film of TiO_2 nanotube arrays is amorphous. Post-annealing of the amorphous

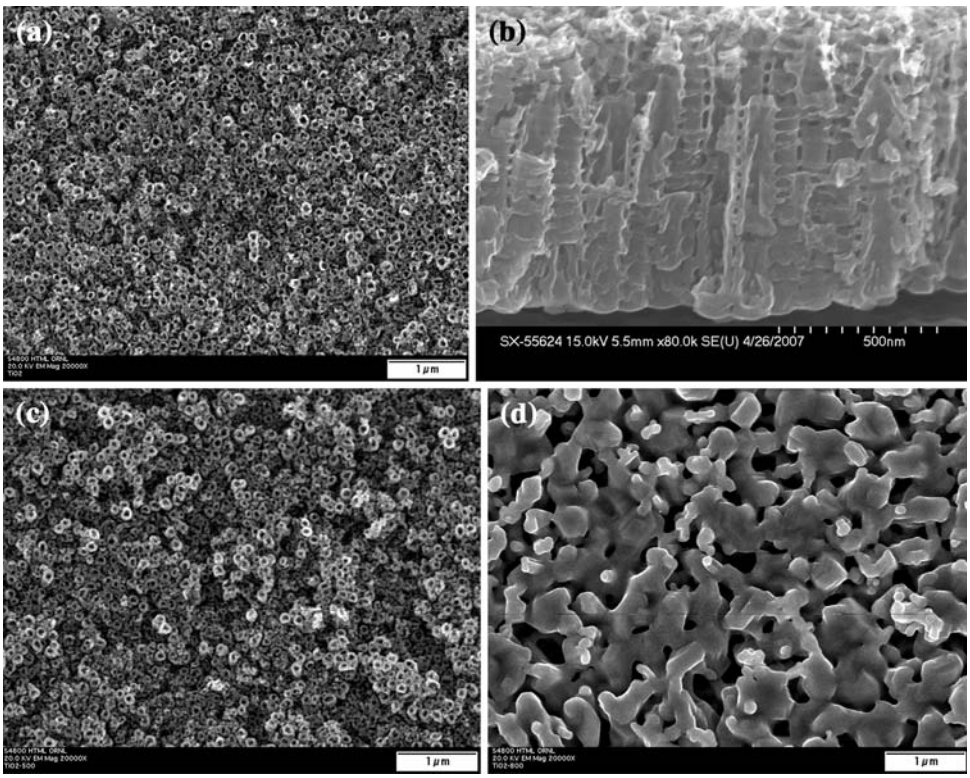

Fig. 2 Top and cross-sectional scanning electron microscope images of TiO_2 nanotubes. Surface of the anodized TiO_2: **a** as-synthesized, **b** cross-sectional view, **c** annealed at 500 °C in Ar for 30 min, and **d** annealed at 800 °C in Ar for 30 min

films at different temperatures under controlled atmospheres produced crystalline phases of anatase and rutile. Nucleation and growth characteristics of the anodized TiO_2 films are shown in Figs. 3 and 4. The nucleation of anatase TiO_2 starts at 400 °C and remains the same up to 700 °C, when the rutile phase starts to nucleate in the presence of the anatase phase. With an increase in the temperature, the

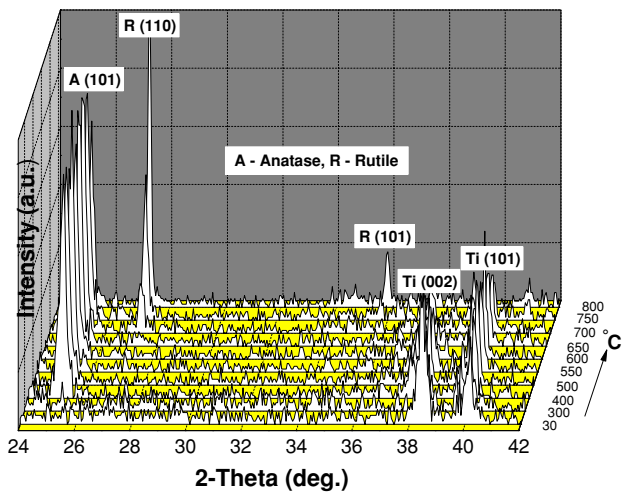

Fig. 3 In situ high temperature X-ray diffraction to monitor the nucleation and growth of crystalline phases in an anodized TiO_2 film at various annealing temperatures

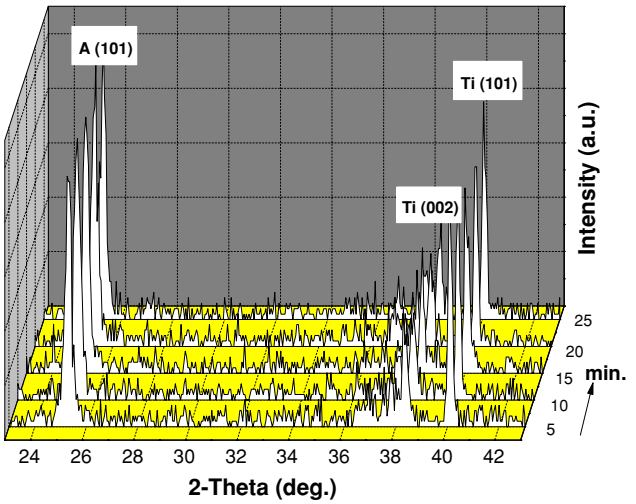

Fig. 4 High temperature X-ray diffraction analysis on phase transformation and growth with time at a constant temperature. Both titanium (Ti) and anatase (A) phases are clearly indexed

rutile phase becomes dominant over the anatase phase. When the TiO_2 sample was heat-treated directly at 500 °C, the nucleation of the anatase phase was instantaneous, and the intensity saturation occurred within 5 min (Fig. 4). With an increase in the heat treatment time, the anatase phase remained stable without the formation of any other secondary phases.

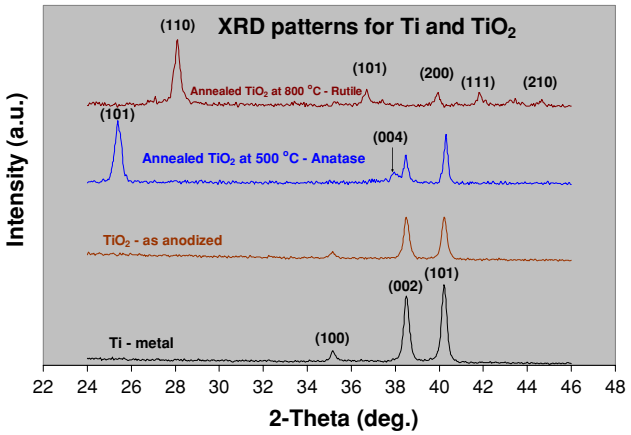

Fig. 5 Powder X-ray diffraction patterns obtained on the Ti metal, anodized TiO_2 (ATO), and annealed ATO samples

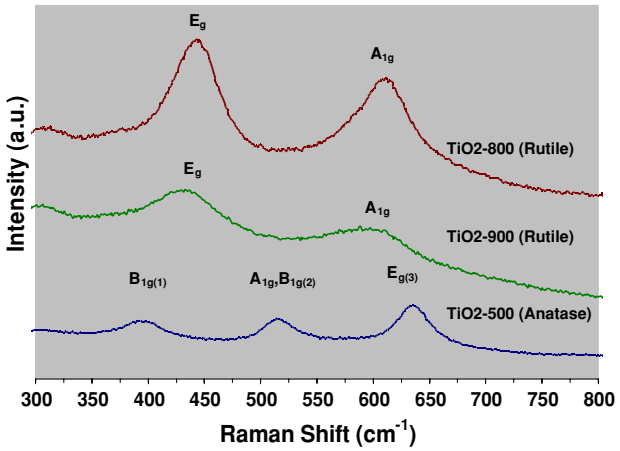

Fig. 6 Raman spectroscopy of annealed anodized TiO_2 samples. All the peaks are assigned with the active modes

Structure analysis by XRD

Room temperature XRD patterns were collected for the starting as-received titanium metal foil, as-anodized TiO_2, and annealed TiO_2 at 500 °C and 800 °C under argon atmospheres. The heating rate was 300 °C/min, so the time to reach 500 °C and 800 °C were approximately 2 and 3 min, respectively, and the total hold time at each target temperature was 1 h in both the cases. The as-received metal foil is polycrystalline in nature with a slight (002) orientation that can be seen in Fig. 5. It is clear from Fig. 5 that the as-anodized TiO_2 is amorphous; however, when heat-treated at 500 °C, a pure polycrystalline anatase TiO_2 phase evolves. A pure rutile TiO_2 phase was observed after heat treatment at 800 °C, which indicates that the TiO_2 structure can be controlled through manipulation of the heat treatment procedure, temperature, and gas atmosphere.

Raman spectral analysis

The anatase TiO_2 has six Raman active modes in the vibrational spectrum: $A_{1g} + 2B_{1g} + 3E_g$ [20–22]. From the single-crystal data, the following allowed bands were determined: 144 cm^{-1} (E_g), 197 cm^{-1} (E_g), 399 cm^{-1} (B_{1g}), 513 cm^{-1} (A_{1g}), 519 cm^{-1} (B_{1g}), and 639 cm^{-1} (E_g). By contrast, rutile TiO_2 has four Raman active modes: $A_{1g} + B_{1g} + B_{2g} + E_g$. From the single-crystal data, the following allowed bands were determined: 143 cm^{-1} (B_{1g}), 447 cm^{-1} (E_g), 612 cm^{-1} (A_{1g}), and 826 cm^{-1} (B_{2g}) [20–22]. Figure 5 compares Raman spectra obtained on the ATO after annealing at 500 °C, 800 °C, and 900 °C in pure argon. Samples annealed at 500 °C confirmed the presence of anatase phase (four allowed modes in the range of 300–800 cm^{-1}). Similarly, samples annealed at 800 °C and 900 °C confirmed the presence of a rutile phase (two allowed modes in the range of 300–800 cm^{-1}). These results are in good agreement with XRD data obtained on the samples and thus provide direct evidence of the phase transformation from anatase (at 500 °C) to rutile (at 800 °C and 900 °C) in the annealed ATO samples. The peak broadening in some of the samples could be due to the decreased crystalline sizes for these vibrational modes (see Fig. 6).

The variation of structure with temperature has been studied by Varghese et al. [10] who reported that the nanotube structure changes during the phase transition of amorphous to anatase and anatase to rutile by a temperature increase. Anatase is obtained from the amorphous phase at about 280 °C. It was reported that at about 400 °C, anatase crystals began to transform into rutile and, at about 580 °C, the transformation was complete. This transformation is accompanied by shrinking of the nanotube size. After this temperature, the authors found that the nanotube structure collapses into a random porous material. Our results confirmed these findings [7].

Electrochemical measurements

In the cases of rutile and anatase films, a significant change in the color of the anode surfaces was observed in all the electrochemical characterization experiments. The surface of the electrodes turned dark purple after photoillumination. This change was negligible in the case of amorphous films. The purple color persisted even after the experiments and could only be removed by vigorous polishing of the electrode. The reason for the color change is believed to be due to electron excitations in transition metals (to *d* orbitals), which are known to produce strong colorations and/or color changes.

The variation of measured current with increasing applied voltages for different films under UV illumination is shown in Fig. 7. The photocurrent density values

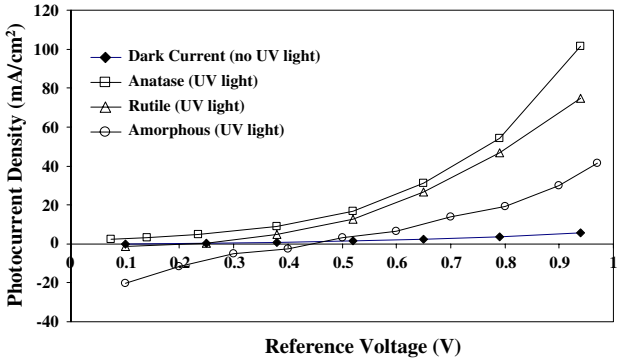

Fig. 7 Current variation versus applied voltage difference for anatase, rutile, and amorphous films (Line segments are used to connect consecutive data points)

determined with anode illumination (photocurrent) showed only a slight increase with respect to the values measured without illumination (dark current) for the amorphous material. The photocurrent values increased as the applied potential increased for all the materials. Anatase films showed the highest current increase at all applied voltages, followed by the rutile films, the amorphous films showed only a small increase.

Figure 8 shows the influence of light power intensity on the photocurrent values. Nominal light intensity values are used in the figure. The equivalent light densities are shown in Table 1. In the case of anatase, higher light powers generated higher photocurrent values at high applied voltages. However, the measured photocurrent results are similar at low applied voltages. This observation coincides with the results of Torres et al. [6], who postulated that, at lower voltages, the photocurrent is controlled by the internal characteristics of the material and not by the externally applied voltage. Similar results were measured for rutile films as well. At high photocurrent conditions, the presence of gas bubbles was observed on the surfaces of

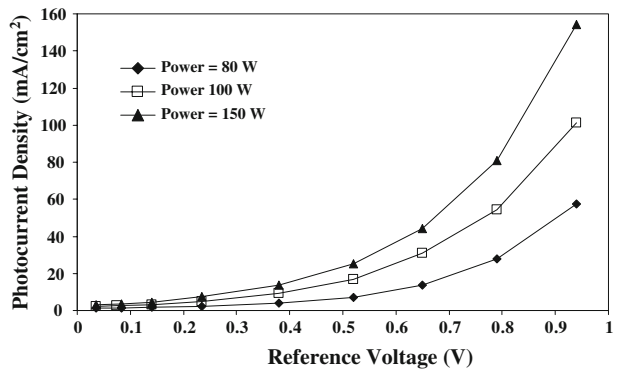

Fig. 8 Influence of light power on efficiency as a function of applied reference voltage for anatase films (Line segments are used to connect consecutive data points)

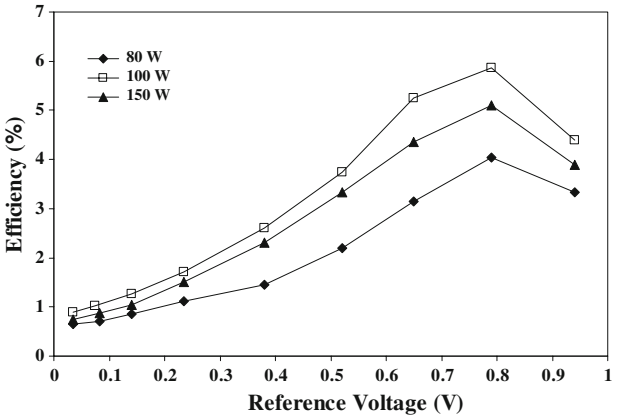

Fig. 9 Influence of light power on efficiency as a function of applied reference voltage for anatase films (Line segments are used to connect consecutive data points)

the Pt electrodes. In case of long experimental runs (more than 3 h), the volume of gas generated was determined, and simple tests showed that the gas was hydrogen.

Figure 9 shows the efficiency calculated using Eq. 3 for anatase films under different light intensities. The efficiency curves show a maximum for all the light intensity values. The value of the efficiency increases as the incident photon energy increases. The maximum values determined for the anatase phase were approximately 5.9%. In the case of rutile, the maximum efficiency value was determined to be 3.8%. The maximum was located at approximately 0.8 V for lamp nominal powers of 80, 100, and 150 W. The measurements conducted at a nominal power of 100 W ($I_o = 231$ mW/cm^2) showed the highest efficiencies followed by the 150 W measurements. All the values are applied voltages relative to the reference Ag/AgCl electrode.

The efficiency values shown in Fig. 9 are below values reported in literature for nitrogen doped titania films (Mor et al. [2], Khan et al. [7]). In this work light scattering through the walls of the electrochemical cell could provoke a smaller 'effective' light intensity on the electrode.

Mor et al. [2] reported an efficiency of about 12.25% obtained for titanium dioxide samples annealed in the range of 580–620 °C. The authors proposed that the increase in photocurrent and efficiency are due to the increased crystallinity of the nanotube-walls, with the reduction of the amorphous regions and grain boundaries [2]. Khan et al. [7]) reported a maximum photoconversion efficiency of 8.35% using a chemically modified n-TiO_2 produced by pyrolysis of a titanium metal sheet. The authors claimed that carbon atoms replaced some of the oxygen lattice atoms producing absorption of light at wavelengths below 535 nm and reducing the material band gap energy to 2.32 eV vs. 3 eV in rutile and 3.2 eV in anatase.

It is widely accepted in the open literature that rutile exhibits lower photocatalytic activity than anatase [23–27]. This effect is generally attributed to differences in the electronic structure and not to differences in surface area values. The different behavior of rutile and anatase was initially attributed to the different position of the conduction-band (more positive for rutile) and to the higher recombination velocity of electron-hole pairs photoproduced in rutile [23, 24]. Other authors [25] postulated that the photocatalytic activity of different surfaces is influenced both by defect concentration and by the atomic makeup of the states close to the Fermi level. Under identical surface preparations, the 101 anatase surface has stronger defect-state intensity relative to the valence band maximum (VBM) than the equivalent 110 rutile surface. In terms of the atomic character of the states close to the Fermi level, the anatase 101 surface is different from rutile 110 surfaces, in that it shows markedly less Ti 3*d* or 4*sp* character in the states around the VBM. This in turn means that the states at the conduction-band minimum should be of quite pure Ti 3*d* character with little mixing with O 2*p*. This conclusion leads to efficient localization of the conduction-band electron created by photoabsorption in a state of Ti^{3+} character preventing hole-electron recombination [25].

Conclusions

Titanium-oxide nanotube arrays in the form of films on the surface of titanium have been synthesized by anodization of titanium metal foil in HF-free aqueous solutions. An as-prepared ATO film is amorphous; however, it becomes anatase with maintained nanotube array morphology after being annealed at 500 °C in an argon atmosphere. At 800 °C, a pure rutile crystalline phase can be obtained, but with the loss of nanotube array morphology. Application of UV light produced a significant increase in the measured photocurrent values for both the anatase and the rutile films. Anatase films showed the highest increase in photocurrent generation. The interaction between the TiO_2 nanotubes at the anode and the incident UV light was confirmed by the color change of the electrode. Anatase films showed the highest efficiency of all the tested materials, about 5.9%. Rutile films showed a maximum value of 3.8%. These results demonstrate that one can use light to generate photocurrent and produce hydrogen by water splitting.

Acknowledgements This work was supported by the Department of Energy, Office of Basic Energy Sciences, Department of Materials Science and Engineering Program and by the Laboratory Directed Research and Development (LDRD) program of ORNL. ORNL is managed by UT-Battelle, LLC, for the US Department of Energy, under contract no. DE-AC05-00OR22725.

References

1. Grimes CA (2007) J Mater Chem 17:1451
2. Mor GK, Varghese OK, Paulose M, Shankar K, Grimes CA (2006) Sol Energ Mater Sol Cells 90:2011
3. Bolton JR (1996) Sol Energy 57:37
4. Fujishima A, Honda K (1972) Nature 238:37
5. Glasscock JA, Barnes PRF, Plumb IC, Bendavid A, Martin PJ (2006). In: Vayssieres L (ed) Solar hydrogen and nanotechnology. Proceedings of the SPIE, vol 6340, pp 63400
6. Torres RG, Gemma L, Torbjörn LJ, Granqvist C-G, Lindquist SE (2004) J Phys Chem B 108(19):5995
7. Khan SUM, Al-Shahry M, Ingler WB Jr (2002) Science 297:2243
8. Lin C-L, Chien S-H, Chao J-H, Sheu C-Y, Huang Y-J, Tsai C-H (2002) Catal Lett 80:153
9. Park JH, Park OO, Kim S (2006) Appl Phys Lett 89:163106
10. Varghese OK, Gong D, Paulose M, Grimes CA, Dickey EC (2003) J Mater Res 18:156
11. Varghese OK, Mor GK, Grimes CA, Paulose M (2004) J Nanosci Nanotechnol 4:733
12. Mor GK, Varghese OK, Pishko MV, Grimes CA (2004) J Mater Res 19:628
13. Kasuga T, Hiramatsu M, Hirano M, Hoson A (1997) J Mater Res 12:607
14. Dagan G, Tomkiewicz M (1993) J Phys Chem 97:12651
15. Yang BC, Uchida M, Kim HM, Zhang XD, Kokubo T (2004) Biomaterials 25:1003
16. Sul YT, Johansson CB, Jeong Y, Albrektsson T (2001) Med Eng Phys 23:329
17. Gong D, Grimes CA, Varghese OK, Dickey EC (2001) J Mater Res 16:3331
18. Beranek R, Hildebrand H, Schmuki P (2003) Electrochem Solid State Lett 6:B12
19. Ruan CM, Wang W, Gu B (2006) Anal Chim Acta 576:114
20. Chen X, Mao SS (2007) Chem Rev 107:2891
21. Giolli C, Borgioli F, Credi A, Di Fabio A, Fossati A, Miranda MM, Parmeggiani S, Rizzi G, Scrivani A, Troglio S, Tolstoguzov A, Zoppi A, Bardi U (2007) Surf Coat Technol 202:13
22. Orendorz A, Brodyanski A, Losch J, Bai LH, Chen ZH, Le YK, Ziegler C, Gnaser H (2007) Surf Sci 601:4390
23. Serpone N, Pelizzetti E (1989) Photocatalysis fundamentals and applications. Wiley & Sons, New York
24. Schiavello M (ed) (1988) Photocatalysis and environment trends and applications. Kluwer Academic, Dordrecht
25. Thomas AG, Flavell WR, Mallick AK, Kumarasinghe AR, Tsoutsou D, Khan N, Chatwin C, Rayner S, Smith GC, Stockbauer RL, Warren S, Johal TK, Patel S, Holland D, Taleb A, Wiame F (2007) Phys Rev B 75(1–12):035105
26. Sciafani A, Herrmann JM (1996) J Phys Chem 100:13655
27. Chuan X-Y, Lu AH, Chen J, Li N, Guo YJ (2008) Mineral Petrol 93:143